10 The Exchange Integral and Exchange Constant

The classical expression for the exchange energy, valid by analogy with the quantum results, for an atom i coupled with nearest neighbour atoms j, is the sum over the neighbours of

$$W_{ij} = -2\mathcal{J}_{ij}\mathbf{S}_i \cdot \mathbf{S}_j \tag{200}$$

the factor of 2 being arbitrary but usually included. $\mathcal{J}$ is known as the exchange parameter. Assuming that the exchange is isotropic and that all the $\mathcal{J}_{ij} = \mathcal{J}$,

$$W_{ij} = -2\mathcal{J}S_iS_j\cos\varphi_{ij} \doteq \mathcal{J}S^2\varphi_{ij}^2 \tag{201}$$

with all $S_i = S$ (for identical atoms), using $\cos 2\varphi = 2\cos^2\varphi - 1$, assuming small angles φ_{ij} between neighbouring spins and dropping constant terms. A more general expression for the energy for a unit cell of a simple cubic, f.c.c. or b.c.c. structure is obtained on carrying out the summations as

$$W = 2\mathcal{J}Sa^2\left[(\nabla\alpha_1)^2 + (\nabla\alpha_2)^2 + (\nabla\alpha_3)^2\right] \tag{202}$$

in terms of the direction cosines α_1, α_2, α_3 relating the spin directions to rectangular coordinate axes.

An important situation is that in which the spins remain parallel within each of a set of neighbouring planes in the crystals with the common orientation changing from plane to plane, as illustrated for complete rotation in four equal steps in Figure 1.56: usually a great

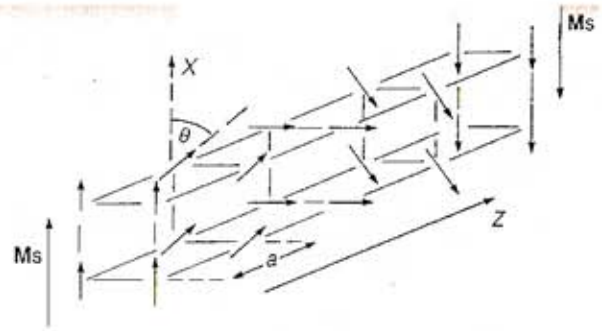

Figure 1.56 All the spins in planes ∥ OXY are assumed parallel. In the general case n (= 4 here) is very large, θ can be taken to be continuous and $\partial\theta/\partial z$ is not constant

number, n, of steps is appropriate. For a simple cubic lattice $a \times a \times a$ there are $1/a^2$ atoms per unit area of plane and the exchange energy per unit area is

$$E = n \times \frac{1}{a^2} \times \mathcal{J}S^2\frac{\pi^2}{n^2} \propto \frac{1}{n} \tag{203}$$

summing equal terms over the n planes involved with all $\varphi_{ij} = \pi/n$. The more gradual the rotation, i.e. the larger n becomes, the lower is the energy.

More generally, if θ is the angle between the common spin direction in the plane positioned along OZ as in Figure 1.56 and a reference axis OX, the change in θ between planes is $a(\partial\theta/\partial z)$ and the energy per spin pair is

$$W = \mathcal{J}S^2a^2\left(\frac{\partial\theta}{\partial z}\right)^2$$

The energy per unit area (for the simple cubic lattice) is thus

$$E = \int_{-\infty}^{\infty}\frac{\mathcal{J}S^2}{a}\left(\frac{\partial\theta}{\partial z}\right)^2 \mathrm{d}z = A\int_{-\infty}^{\infty}\left(\frac{\partial\theta}{\partial z}\right)^2 \mathrm{d}z, \qquad \text{where } A = \frac{\mathcal{J}S^2}{a} \tag{204}$$

The same expression is seen to apply for other cubic lattices with

$$A = \frac{2\mathcal{J}S^2}{a} \qquad \text{(b.c.c.)} \tag{205}$$

$$A = \frac{4\mathcal{J}S^2}{a} \qquad \text{(f.c.c)} \tag{206}$$

A is the exchange constant and is important in characterizing domain walls as in Section 12.2.

11 Magnetocrystalline Anisotropy and Magnetostriction

The tendency for M_s to lie along an easy axis can be described using the magnetocrystalline anisotropy constants K_i. For a purely uniaxial crystal, with no anisotropy normal to the single

easy axis, an approximate expression for the anisotropy energy density is

$$E_K = K \sin^2 \theta \tag{207}$$

θ being the angle between $\mathbf{M}_s$ and a coordinate axis parallel to the easy axis. E_K is zero when $\mathbf{M}_s$ is parallel or antiparallel to the arbitrarily directed coordinate axis and maximum for $\theta = \pi/2$, i.e. has appropriate symmetry. This would apply with other even terms and

$$E_K = K_1 \sin^2 \theta + K_2 \sin^4 \theta + \cdots \tag{208}$$

is more general, the number of terms chosen depending on the accuracy with which measurements can be made. For cobalt at room temperature (the K_i vary rapidly with temperature),

$$K_1 = 4.1 \times 10^5 \mathrm{J\,m^{-3}}, \qquad K_2 = 1.0 \times 10^5 \mathrm{J\,m^{-3}}$$

and it is clear that the simple equation (207) can be used reasonably, particularly for small deviations of $\mathbf{M}_s$ from the easy axis for this and in fact other materials. Exact measurements of the torque on $\mathbf{M}_s$ as a crystal is rotated in large saturating fields reveal a small anisotropy in the basal plane accounted for by

$$E_K = K_1^{\mathrm{u}} \sin^2 \theta + K_2^{\mathrm{u}} \sin^4 \theta + K_3^{\mathrm{u}} \sin^6 \theta + K_3 \sin^6 \theta \cos^4 \phi \tag{209}$$

with θ and ϕ the polar angle (as above) and azimuthal angle w.r.t. the c axis. The superscript distinguishes the uniaxial terms. This E_K is minimum, for hexagonal crystals, with $M_s \parallel$ [0001] for

$$K_1 + K_2 > 0 \qquad \text{and} \qquad K_1 > 0$$

However, for

$$0 \leqslant K_1 < -K_2 \qquad \text{or} \qquad -K_1 > 2K_2 \qquad \text{and} \qquad K_1 < 0$$

E_K is lowest when $\mathbf{M}_s$ lies in the (0001) basal plane, giving an easy-plane or planar material.

For cubic crystals an expression with appropriate symmetry is (truncated)

$$E_K = K_1(\alpha_1^2\alpha_2^2 + \alpha_2^2\alpha_3^2 + \alpha_3^2\alpha_1^2) + K_2(\alpha_1^2\alpha_2^2\alpha_3^2) \tag{210}$$

In the case that

$$K_1 > 0 \qquad \text{and} \qquad K_1 > -\tfrac{1}{9}K_2$$

the [100] axes are the easy axes and if

$$K_1 < 0 \qquad \text{and} \qquad K_1 < -\tfrac{4}{9}K_2 \qquad \text{or} \qquad 0 < K_1 < -\tfrac{1}{9}K_2$$

the [111]'s are easy axes. However, it is usually adequate to accept that, formally,

$$K_1 > 0 \sim [100], \qquad K_1 < 0 \sim [111] \text{ easy axes}$$

K_1 is positive for iron and negative for nickel.

Anisotropy fields may be regarded as those fields which, when applied along an easy axis, give the same torques as those corresponding to the anisotropy and thus may be taken to represent the anisotropy. The correspondence only applies when the magnetization deviates from an easy direction only by a small angle $\Delta\theta$ for which $\sin \Delta\theta = \Delta\theta$ is acceptable and the torque is

$$T_{H_K} = -\frac{\partial}{\partial\theta} E_{H_K} = -\frac{\partial}{\partial\theta} \mu_0 H_K M_s \cos\theta = \mu_0 H_K M_s \Delta\theta$$

The torque due to the anisotropy can be expanded and truncated as

$$T_K = \frac{\partial E_K}{\partial\theta} = \left(\frac{\partial E_K}{\partial\theta}\right)_{\theta=0} + \left(\frac{\partial^2 E_K}{\partial\theta^2}\right)_{\theta=0} \Delta\theta = \left(\frac{\partial^2 E_K}{\partial\theta^2}\right)_{\theta=0} \Delta\theta$$

since $\partial E_K/\partial\theta = 0$ when M_s lies along an easy direction. Equating the two,

$$H_K = \frac{1}{\mu_0 M_s}\left(\frac{\partial^2 E_K}{\partial\theta^2}\right)_{\theta=0} \tag{211}$$

(H_A is often used to denote a general anisotropy field with H_K used to indicate that magnetocrystalline anisotropy is specifically considered.) Using equation (208),

$$H_K = \frac{1}{\mu_0 M_s}\left[2K_1(-\sin^2\theta + \cos^2\theta) + \frac{1}{\mu_0 M_s} 4K_2(-\sin^4\theta + 3\sin^2\theta\cos^2\theta)\right]_{\theta=0}$$
$$= \frac{2K_1}{\mu_0 M_s} \tag{212}$$

Similarly, it can be shown that

$$H_K = \frac{2K_1}{\mu_0 M_s} \qquad \text{[100] easy direction} \tag{213}$$

$$H_K = -\frac{(\frac{4}{3}K_1 + \frac{4}{9}K_2)}{\mu_0 M_s} \qquad \text{[111] easy direction} \tag{214}$$

There is no lower limit to H_K since, for certain materials (e.g. certain Ni–Fe alloys), $K_1 \to 0$. The wide range of values is indicated by

Iron: 45, Cobalt: 4200, $SmCo_5$: 20 000 $\mathrm{kA\,m^{-1}}$ and other values are given in Chapter 5.

Magnetostrictive strains are anisotropic or there would be no saturation magnetostrictive length change δl observed as the $\mathbf{M}_s$ vectors rotate to give saturation, from an initial ideal demagnetized state with equal volumes magnetized along each of the easy directions. This effect is described by the saturation magnetostriction coefficient $\lambda_s = \delta l/l$. Typically, $\lambda_s = -10$ to -100×10^{-6} but the anisotropic coefficients may be positive or negative. The measured deformation $\lambda - \lambda_d$, with λ_d for demagnetization, depends upon the direction cosines $\alpha_1, \alpha_2, \alpha_3$ specifying the direction along which $\mathbf{M}_s$ is eventually aligned and the β_i specifying the direction along which the measurement is made. Usually the two coincide and $\lambda - \lambda_d$ is designated $\lambda_{100}(\lambda_{111})$ when the direction is a cube edge (diagonal), etc. The λ_d themselves can be expressed (e.g. [20]) as

$$\lambda_d = B_0 + \tfrac{1}{3}B_1 + \tfrac{1}{3}B_4$$

for [100] easy directions, $K_1 > 0$ as for iron, or

$$\lambda_d = B_0 + \tfrac{1}{3}B_1 + \tfrac{1}{3}B_3 + \tfrac{1}{6}B_4$$

for [111] easy directions, $K_1 < 0$ as for nickel, and further

$$\lambda_{100} = \tfrac{2}{3}B_1 + \tfrac{2}{3}B_4$$
$$\lambda_{111} = \tfrac{1}{3}B_2 + \tfrac{1}{3}(B_3 - \tfrac{2}{3}B_4) + \tfrac{1}{9}B_5$$

for iron, etc., and

$$\lambda_{100} = \tfrac{2}{3}B_1 - \tfrac{1}{3}B_3 + \tfrac{8}{9}B_4$$
$$\lambda_{111} = \tfrac{1}{3}B_2 + \tfrac{1}{9}B_5$$

for nickel, etc. The B_i are magnetostriction constants related to S_{ij} and L_i, which are respectively the elastic compliance moduli and the magnetoelastic coupling constants. The deformation of any cubic crystal can be written in an approximation (for powers of α_i up to the second) as

$$\frac{\delta l}{l} = \tfrac{2}{3}\lambda_{100}(\alpha_1^2\beta_1^2 + \alpha_2^2\beta_2^2 + \alpha_3^2\beta_3^2 - \tfrac{1}{3}) + 3\lambda_{111}(\alpha_1\alpha_2\beta_1\beta_2 + \alpha_2\alpha_3\beta_2\beta_3 + \alpha_1\alpha_3\beta_1\beta_3)$$

For a random polycrystal the longitudinal magnetostriction is obtained by averaging (with all $\alpha_i = \beta_i$) as

$$\lambda = \tfrac{2}{5}\lambda_{100} + \tfrac{3}{5}\lambda_{111}$$

For uniaxial crystals Bozorth [21] used

$$\frac{\partial l}{l} = k_1(\alpha_1^2 - 1)\beta_1^2 + k_2(\alpha_2^2\beta_2^2 + \alpha_3^2\beta_3^2) + k_3(\alpha_3^2\beta_2^2 + \alpha_2^2\beta_3^2) + 2(k_2 - k_3)\alpha_2\alpha_3\beta_2\beta_3$$
$$+ 2k_4\alpha_1\beta_1(\alpha_3\beta_3 + \alpha_2\beta_2)$$

with $k_1 = -110$, $k_2 = -45$, $k_3 = -95$, $k_4 = -235$, (all $\times 10^{-6}$) for cobalt.

12 Magenetostatic Energy and Domain Walls

12.1 Magnetostatic Energy and Domains

The state in which a ferromagnetic is usually found is one of zero magnetization. In a polycrystal this could be because each crystallite is uniformly magnetized, but the directions of $\mathbf{M}_s$ are distributed randomly. More generally, and necessarily in single crystals, it may be inferred that the crystal, or each crystallite, is divided into a number of regions or domains of volume v_i each with uniform magnetization of magnitude $M_i = M_s$ such that in the demagnetized state $\sum v_i M_j^i = 0$, for $j = x, y, z$. Obvious minimal examples are shown in Figure 1.57. The domain boundaries or domain walls are sheets of thickness usually much less than the domain width, in which the magnetization rotates (usually) gradually between the directions in the two domains, the width and surface energy density of the walls being calculable in terms of A, K and the wall orientations.

The tendency towards demagnetization by the formation of domains accords with the consequent reduction of the total energy, initially considered as the sum of the magnetostatic self-energy and the domain wall energy (for uniaxial crystals with $\mathbf{M}$ parallel to easy directions forming 180° domains). The magnetostatic energy E_m may be considered as that

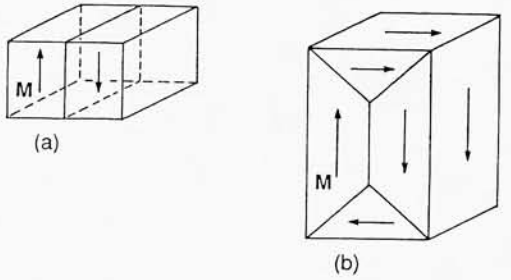

Figure 1.57 Rudimentary 180° domain structures in a uniaxial crystal (a) and in a cubic (iron) crystal (b) with 90° domains affording flux closure and minimal magnetostatic energy

required to bring up the constituent dipoles from infinity, i.e. as the energy of formation; as discussed in Chapter 4, it is calculated by evaluating the integral of the product of pole density and potential over the specimen, the potential being that generated by the magnetization. Alternatively and equivalently,

$$E_m = \tfrac{1}{2}\int \mu_0 \mathbf{H}_d \cdot \mathbf{M}\, dv \tag{215}$$

over the specimen volume, where $\mathbf{H}_d$ is the internal demagnetizing field.

If the specimen has the shape of an ellipsoid of revolution, $\mathbf{H}_d$ is uniform if $\mathbf{M}$ is uniform. For oblate or prolate spheroids with $\mathbf{M}$ parallel to a principal direction [22],

$$\mathbf{H}_d = -N\mathbf{M}$$

with N a (positive) dimensionless demagnetizing factor. For ellipsoids of revolution (Figure 1.58 with $b = c$) with $\mathbf{M} \parallel$ the long axis a (prolate spheroids)

$$N_a = \frac{1}{q^2 - 1}\left[\frac{q}{\sqrt{q^2 - 1}}\ln(q + \sqrt{q^2 - 1} - 1)\right] \to \frac{1}{q^2}(\ln 2q - 1) \tag{216}$$

with $q = a/b$ and the second expression for $q \gg 1$. For flat ellipsoids with two long axes a and b nearly equal and much greater than the short axis c,

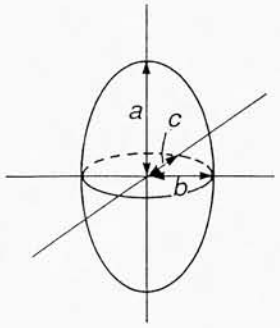

Figure 1.58 A general ellipsoid with Cartesian axes taken to coincide with the principal axes

$$N_a = \frac{\pi}{4}\frac{c}{a}\left[1 - \tfrac{1}{4}\frac{a-b}{a} - \tfrac{3}{16}\left(\frac{a-b}{a}\right)^2\right]$$
$$N_b = \frac{\pi}{4}\frac{c}{a}\left[1 + \tfrac{5}{4}\frac{a-b}{a} + \tfrac{21}{16}\left(\frac{a-b}{a}\right)^2\right] \qquad (217)$$

For oblate spheroids with **M** parallel to the circular plane,

$$N = \tfrac{1}{2}\left[\frac{q^2}{(q^2-1)^{3/2}}\sin^{-1}\frac{\sqrt{q^2-1}}{q} - \frac{1}{q^2-1}\right] \qquad (218)$$

with q = diameter/thickness.

The relation

$$N_a + N_b + N_c = 1 \qquad (219)$$

applies to the three factors appropriate to the three axes of an ellipsoid. Thus, by symmetry, for a sphere

$$N_a = N_b = N_c = \tfrac{1}{3} \qquad (220)$$

For a long cylinder with **M** ∥ the long axis a, $N_a = 0$ because the 'end poles' are distant and thus

$$N_b = N_c = \tfrac{1}{2} \qquad (221)$$

which applies when **M** is normal to the long axis. For a thin plate, considered as an ellipsoid with $k = 0$, two factors are zero and $N_c = 1$, as inferred previously.

If the principal axes of an ellipsoid coincide with the Cartesian axes as in Figure 1.58, the surface poles due to the x component of a generally directed **M** can only give a field ∥ OX, etc., and thus

$$\begin{pmatrix} H_x \\ H_y \\ H_z \end{pmatrix} = \begin{pmatrix} N_b & 0 & 0 \\ 0 & N_c & 0 \\ 0 & 0 & N_a \end{pmatrix}\begin{pmatrix} M_x \\ M_y \\ M_z \end{pmatrix} = \begin{pmatrix} N_{11} & 0 & 0 \\ 0 & N_{22} & 0 \\ 0 & 0 & N_{33} \end{pmatrix}\begin{pmatrix} M_x \\ M_y \\ M_z \end{pmatrix} \qquad (222)$$

If the axes do not coincide it is necessary to take the components of **M** along the ellipsoid axes, find the field components along these axes and then resolve these along OX, OY, OZ so that, formally, $\mathbf{H}_d = \mathbf{NM}$, where **N** is the demagnetizing tensor which is diagonal only in the above special case.

Magnetostatic or demagnetizing energies of short cylinders or rectangular blocks with uniform magnetization are readily calculated numerically and effective demagnetizing factors can be defined in relation to these, or by

$$\bar{N} = -\bar{H}_d/M$$

where $\bar{H}_d$ is the mean demagnetizing field calculated. These can only be used in approximate calculations.

If a cube (or sphere) is divided equally into two domains as in Figure 1.57(a), E_m is halved and if it were divided into a great number of domains, it is clear that H_d and E_m would tend towards zero. However, the wall energy density per unit volume E_w would become very great and an equilibrium domain width is expected to correspond to a minimum of $(E_m + E_w)$. However, since E_m is the energy per unit volume it is easily seen that for particles below a certain critical size it may not be energetically favourable to introduce even a single domain wall and very small particles or crystallites are expected to exhibit 'single-domain behaviour' as noted in Chapter 5, Section 2.1, the single- and two-domain energies are equal at $r = r_c = 9\gamma/(\mu_0 M_s^2)$ and for iron $r_c \approx 1$ nm. γ is the wall energy per unit area.

If the particle size is reduced even further the peak value of W_k as $\mathbf{M}_s$ rotates, e.g. of $K\sin^2\theta \times$ particle volume, may become less than kT at room temperature, say. The energy barriers to rotation become relatively ineffective and the distribution of the magnetic moments of a particle assembly may be given by applying Boltzmann statistics giving superparamagnetic behaviour, discussed in Chapter 5, Section 2.2.

12.2 Domain Walls

The more gradual the rotation of **M** the lower is the exchange energy. If $\mathbf{M}_s$ were arbitrarily pinned at oppositely magnetized faces of a crystal it might be expected that the rotation should occupy the whole specimen. However, this would give a high value of E_K (particularly apparent for a uniaxial crystal) and it is thus expected that a wall with a particular (asymptotic) width $\delta\,(A, K)$ and surface energy $\gamma\,(A, K)$ should be formed. Usually (unless $K \to 0$), $\delta \ll l$, the domain width, and $\delta = 0$ is assumed in calculating E_m.

Taking the rotation to occur along OZ and to be indicated by the single angle $\theta(z)$ as in Figure 1.56 (but with a great number of steps so that θ can be considered as a continuous variable), the anisotropy energy for each layer per unit surface area of wall may be designated $f(\theta)$ and (per unit area)

$$\gamma = \gamma_c + \gamma_K = \int_{-\infty}^{\infty}\left[A\left(\frac{\partial\theta}{\partial z}\right)^2 + f(\theta)\right]\mathrm{d}z \qquad (223)$$

Assuming that $\theta(z)$ is in fact that function which gives the minimum energy and introducing a small change $\delta\theta$, the change in γ is

$$\delta\gamma = \int_{-\infty}^{\infty}\left[2A\frac{\partial\theta}{\partial z}\frac{\partial}{\partial z}\delta\theta + \frac{\partial f(\theta)}{\partial z}\delta\theta\right]\mathrm{d}z \qquad (224)$$

In the usual way it is assumed that the minimum energy (stable configuration) corresponds to $\delta\gamma = 0$. Integrating the first term by parts

$$\int_{-\infty}^{\infty} 2A\frac{\partial\theta}{\partial z}\frac{\partial}{\partial z}\delta\theta\,\mathrm{d}z = \left[2A\frac{\partial\theta}{\partial z}\delta\theta\right]_{-\infty}^{\infty} - \int_{-\infty}^{\infty} 2A\frac{\partial^2\theta}{\partial z^2}\delta\theta\,\mathrm{d}z$$

and assuming **M** to be uniform within the domains, where the limits effectively apply, the first term is zero. The condition $\delta\gamma = 0$ is

$$\int_{-\infty}^{\infty}\left[\frac{\partial f(\theta)}{\partial\theta} - 2A\frac{\partial^2\theta}{\partial z^2}\right]\delta\theta\,\mathrm{d}z = 0$$

and since $\delta\theta$ is arbitrary, this means that

$$\frac{\partial f(\theta)}{\partial\theta} - 2A\frac{\partial^2\theta}{\partial z^2} = 0 \qquad (225)$$

(which could have been written directly as the Euler equation of the one-dimensional variational problem). Multiplying by $\partial\theta/\partial z$ and integrating,

$$f(\theta) = A\left(\frac{\partial\theta}{\partial z}\right)^2, \qquad \mathrm{d}z = \sqrt{A}\frac{\mathrm{d}\theta}{\sqrt{f(\theta)}} \tag{226}$$

[since $\theta = \theta(z)$ only]. Integrating this formally,

$$z = \sqrt{A}\int_0^{\theta}\frac{\mathrm{d}\theta}{\sqrt{f(\theta)}}$$

Noting from the above that the exchange and anisotropy terms are equal,

$$\gamma_{180} = 2\sqrt{A}\int_0^{\pi}\sqrt{f(\theta)}\,\mathrm{d}\theta \tag{227}$$

e.g.

$$\gamma_{180} = 2\sqrt{A}\int_0^{\pi}\sqrt{K}\sin\theta\,\mathrm{d}\theta = 4\sqrt{AK} \qquad \text{(simple uniaxial case)} \tag{228}$$

A typical value of A may be obtained from the Bloch $T^{3/2}$ law as $10^{-11}\,\mathrm{J\,m^{-1}}$, giving ($K = 1.3 \times 10^7\ \mathrm{J\,m^{-3}}$)

$$\gamma_{180}(\mathrm{SmCo_5}) = 46 \times 10^{-3}\ \mathrm{J\,m^{-2}}$$

which is practically an upper limit, with no lower limit since $K \to 0$ may be envisaged.

Taking both z and θ to be zero at the wall centre, $f(\theta) = K\cos^2\theta$ and

$$z = \sqrt{\frac{A}{K}}\int_0^{\theta}\frac{\mathrm{d}\theta}{\cos\theta} = \sqrt{\frac{A}{K}}\ln\tan\left(\frac{\theta}{2}+\frac{\pi}{4}\right) \tag{229}$$

using a standard integral. $\theta(z)$ throughout the 180° wall is as shown in Figure 1.59 with asymptotic approaches to **M** in the bulk of the domains. Truncation may be achieved by extrapolation using $\partial\theta/\partial z$ at the wall centre as shown, giving

$$\delta = \pi\left.\frac{\partial\theta}{\partial z}\right|_{z=0} = \pi\sqrt{\frac{A}{K}} \tag{230}$$

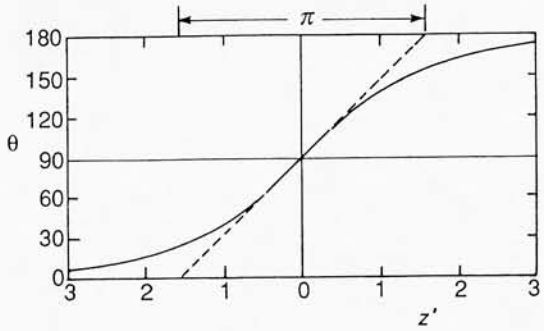

Figure 1.59 The variation of the moment orientation throughout a 180° domain wall

Taking A as before and $K = 4 \times 10^4\ \mathrm{J\,m^{-3}}$ for iron,

$$\delta_{180}(\mathrm{Fe}) = 50\ \mathrm{nm}$$

$$\delta_{180}(\mathrm{SmCo_5}) = 2.8\ \mathrm{nm}$$

For iron the continuum model is justified but for $SmCo_5$ most of the rotation is predicted to occur over a few lattice planes only, and then a small threshold field (intrinsic coercive field) is required to move the wall, even in a perfect crystal [23]. Again, if $K \to 0$ there is no upper limit, but even when efforts are made to achieve $K \approx 0$ in practice (to optimize χ as shown later) a variety of observations indicate that walls with finite though large widths occur.

Even in cubic materials, 180° walls, e.g. between [100] and [$\bar{1}$00] domains, are common but in iron 90° walls separate [100] and [010] domains, for example, and in nickel etc. ($K_1 < 0$) 71° and 109° walls separate domains magnetized along ⟨111⟩ as in Figure 6.3. For a 180° wall in iron with the spins rotating in a (100) plane,

$$\gamma_{180} = 2\sqrt{AK} \tag{231}$$

while for a 90° wall

$$\gamma_{90} = \sqrt{AK} \tag{232}$$

The spins at the centre of a 180° wall can follow an easy direction. Further results are given by Lilley [24], following Landau and Lifshitz [25, 26], by Néel [27] and by Kaczer [28].

Where walls intersect surfaces ∥ **M** narrow strips of pole density may form which can attract the fine particles (~ 10 nm diameter) of a colloid of magnetite, such colloids or

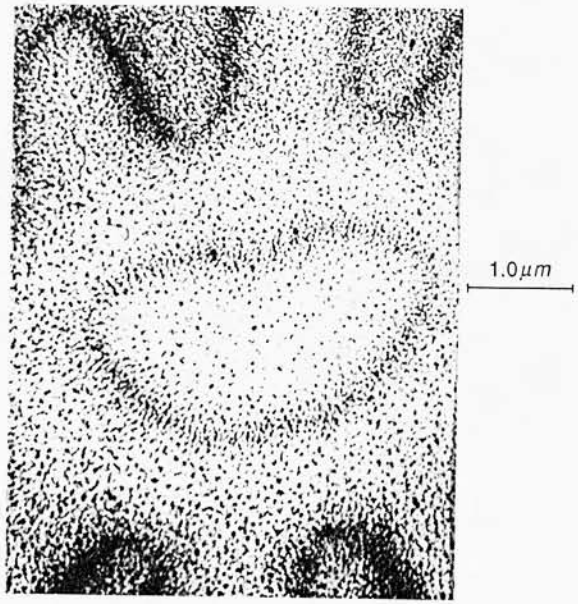

Figure 1.60 The formation of chains of minute magnetite particles in the strong stray fields above the intersection of a narrow 180° domain wall with a crystal surface ⊥ $\mathbf{M}_s$ of barium ferrite (giving rise to interesting optical effects in a polarizing microscope)

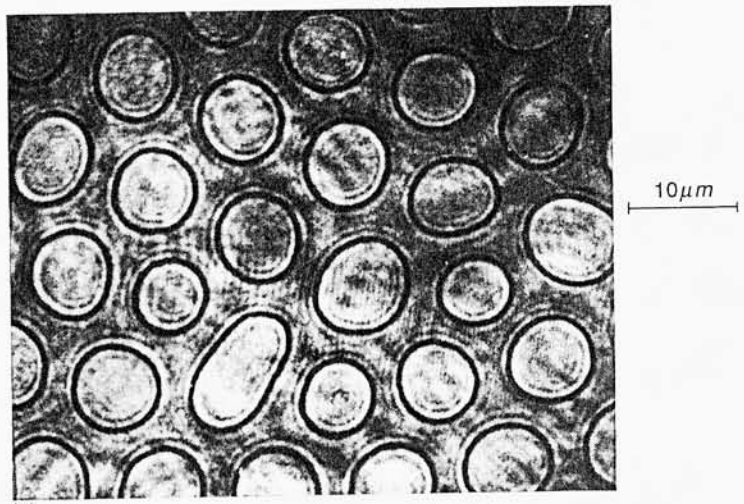

(a)

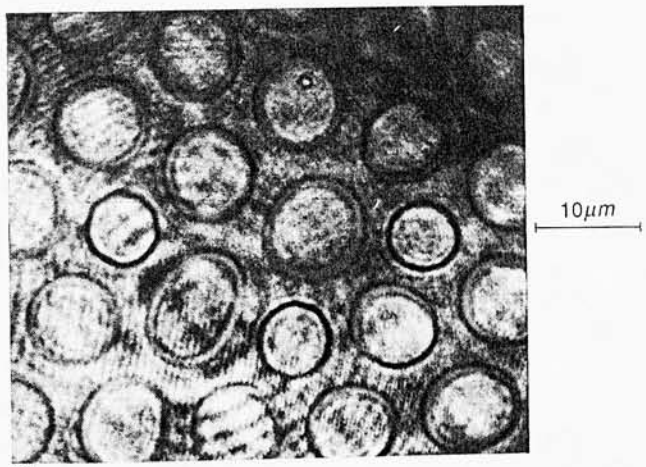

(b)

Figure 1.61 (a) An array of 180° cylindrical, bubble, domains with M normal to the surface of a thin single-crystal film of $Tb_{0.3}\ Eu_{0.3}\ Y_{2.4}\ Ga_{1.1}\ Fe_{3.9}\ O_{12}$ revealed by the Faraday effect using a laser source (see Chapter 6). (b) In a 50 Hz, 15 Oe field the walls of the larger domains are seen to oscillate freely but those of the smaller domains, assumed to have a complex and high energy (Bloch line) structure, remain static [29]

'ferrofluids' being readily prepared. Strong field gradients arise above the intersections of walls with surfaces $\perp$ **M** and lines of particles may be formed to visualize these walls as in Figure 1.60. Figure 1.61 [29] shows 180° walls in a uniaxial garnet crystal, revealed by the Faraday effect (Chapter 5); the caption indicates the complexities that may arise. Reference may be made to specific works on domains [30, 31] and to Chapter 4, Section 2 and Chapter 6, Section 1.

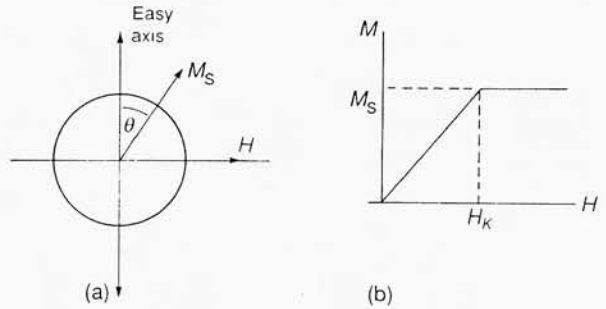

Figure 1.62 For a uniaxial single-domain sphere the equilibrium θ depends in a simple way on the balance of the torques due to the field and the magnetocrystalline anisotropy (a), giving the result in (b) where M is the component of $\mathbf{M}_s$ along **H**

13 Magnetization Processes

13.1 Rotation

For the uniaxial sphere in Figure 1.62 the θ-dependent energy density is $K\sin^2\theta - \mu_0 H M_s \sin\theta$ and equilibrium corresponds to

$$2K\sin\theta\cos\theta - \mu_0 H M_s\cos\theta = 0, \qquad \text{i.e. } \sin\theta = \frac{\mu_0 H M_s}{2K}$$

The magnetization induced in the field direction is

$$M = M_s\sin\theta = \mu_0\frac{H M_s^2}{2K}, \qquad \chi = \frac{M}{H} = \frac{\mu_0 M_s^2}{2K} \tag{233}$$

χ is constant up to saturation at $H = H_K = 2K/(\mu_0 M_s)$ as in Figure 1.62(b). Using two constants it is easy to show that the equation for the equilibrium M is

$$\mu_0 H M_s = 2\frac{M}{M_s}\left[K_1 + 2K_2\left(\frac{M}{M_s}\right)^2\right] \tag{234}$$

from which M and χ for any H can be computed. Curve-fitting $M(H)$ can give estimates of K_1 and K_2. For initial susceptibilities, extrapolated to zero H or measured in very small fields $(M/M_s)^2$ can be ignored and χ is as before.

With a field at angle α to an easy direction the initial susceptibility is

$$\chi_i = \mu_0\frac{M_s^2\sin^2\alpha}{2K} \tag{235}$$

for a uniaxial or cubic, $K_1 > 0$, material. For $K_1 < 0$ the anisotropy energy for small deflections is $E_K = \frac{2}{3}|K_1|\theta^2$, giving

$$\chi_i = \frac{3\mu_0 M_s^2\sin^2\alpha}{4|K_1|} \tag{236}$$

For a random assembly of particles, using $\langle \sin^2 \alpha \rangle = \frac{2}{3}$,

$$\chi_i = \frac{\mu_0 M_s^2}{3K_1} \qquad \text{(uniaxial, cubic } K_1 > 0\text{)} \tag{237}$$

$$\chi_i = \frac{\mu_0 M_s^2}{2K_1} \qquad \text{(cubic, } K_1 < 0\text{)} \tag{238}$$

13.2 Switching: Coherent Reversal

With **H** precisely parallel to an easy axis and antiparallel to $\mathbf{M}_s$, $\mathbf{H} \times \mathbf{M}_s = 0$. If $\mathbf{M}_s$ is displaced by a small angle $\delta\theta$ from the easy axis the anisotropy field concept applies and if $H > 2K/(\mu_0 \mathbf{M}_s)$ the net field is in the direction of **H** and adequate to overcome energy barriers during rotation, i.e. even with $\delta\theta = 0$ the original direction is metastable. Thus it may be inferred that abrupt switching occurs in a reverse field if

$$H = H_c = H_K = \frac{2K}{\mu_0 M_s} \tag{239}$$

This can be confirmed by plotting the energies and torques as H is varied.

The magnetization loop is thus as shown in Figure 1.63. The remanent magnetization remaining after removing a saturating field is $M_r = M_s$. The *coercivity* or *coercive field* H_c, required to give zero magnetization, is in this case the switching field since $M = 0$ is an unstable state.

If **H** is applied at 45° to the easy axis the reader may readily confirm that $\mathbf{M}_s$ rotates reversibly until a discontinuity occurs at a field given by

$$\mu_0 H M_s \sin\frac{\pi}{2} = 2K \sin\frac{\pi}{4}\cos\frac{\pi}{4}, \qquad \text{i.e. } H_c = \frac{K}{\mu_0 M_s}$$

since beyond the corresponding angle the torque due to the field increases with θ and that due to the anisotropy decreases. The loop is as shown in Figure 1.64, after Stoner and Wohlfarth [32].

The dependence of the magnetostatic energy of an ellipsoid of revolution on the angle between **M** and the a axis is shown in Chapter 4 to be the same as that of E_K on the angle between **M** and the (single) easy axis, and with $K_s = \frac{1}{2}\mu_0 M_s^2 (N_b - N_a)$ for the shape

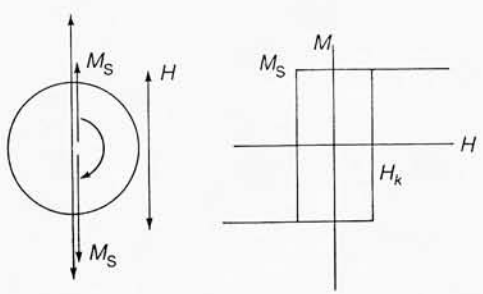

Figure 1.63 **H** ∥ the easy axis gives no torque but discontinuities are expected to occur to give the loop shown

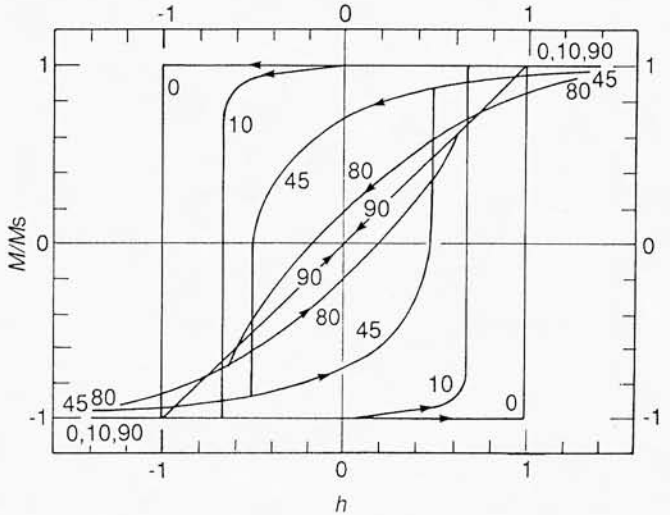

Figure 1.64 A set of 'Stoner–Wohlfarth' loops for the field orientations indicated, given in terms of $h = H/H_K$ or $h = H/H_s$ for either magnetocrystalline or shape anisotropies [32]

anisotropy the simple results applying to crystal anisotropy can be applied to shape effects as, for example,

$$\chi = \frac{\mu_0 M_s^2}{2K_s} = \frac{1}{N_b - N_a}, \qquad H_c = \frac{2K_s}{\mu_0 M_s} = M_s(N_b - N_a) \tag{240}$$

Further, a shape anisotropy field may be derived as before as

$$H_s = M_s(N_b - N_a) \tag{241}$$

and the set of magnetization curves in Figure 1.64 can be given in terms of $h = H/H_A$ with $H_A = H_K$ or $H_A = H_s$, applying equally to either anisotropy. A virtual upper limit to $H_c = H_s$, for very long iron particles, is

$$H_c = (N_b - N_a)M_s = (\tfrac{1}{2} - 0)M_s = 850 \text{ kA m}^{-1}$$

If both types coexist, as in an anisotropic ellipsoid, the sum of the three appropriate energy terms can be minimized to predict the behaviour. If a single easy axis coincides with the a axis of the ellipsoids the two anisotropy fields may be summed. Shape effects can increase or decrease values of H_c due to crystal anisotropy alone.

It has been observed that lattices generally deform when ordering occurs and these deformations are anisotropic and depend on the direction of the magnetization. If an initially demagnetized specimen of length l, with randomly oriented M_s vectors, is magnetized there is a small change of length δl in the direction of magnetization and the magnetostriction coefficient is defined as

$$\lambda = \frac{\delta l}{l} \tag{242}$$

with λ_s for saturation. If the magnetization lies at an angle θ to the direction of measurement of δl it is found that

$$\frac{\delta l}{l} = \tfrac{3}{2}\lambda_s\left(\cos^2\theta - \tfrac{1}{3}\right) \tag{243}$$

If the magnetostrictive deformation occurs in the presence of an applied tensile stress σ, then considering the work done the variable part of the corresponding energy is

$$E_\sigma = -\tfrac{3}{2}\lambda_s\sigma\cos^2\theta = -\tfrac{3}{2}\lambda_s\sigma(1-\sin^2\theta) \tag{244}$$

When $\lambda_s > 0$, E_σ is minimum for $\theta = 0$ and $\theta = 2\pi$ and the magnetization tends to be aligned along the (tensile) stress axis, giving a uniaxial anisotropy analogous to a crystal anisotropy with K replaced by

$$K_\sigma = \tfrac{3}{2}\lambda_s\sigma \tag{245}$$

with an anisotropy field

$$H_\sigma = \frac{3\lambda_s\sigma}{\mu_0 M_s} \tag{246}$$

Most of the principles developed here are relevant to single-domain particles with no domain wall processes involved, and are developed later as appropriate.

13.3 Remanence

For aligned single-domain particles it has been seen that M_r/M_s can be unity. For a randomly oriented assembly of s–d crystallites, if it is assumed that, on removal of a saturating field, $\mathbf{M}_s$ in each crystallite relaxes back to the nearest easy direction, then averaging gives (as shown by Gans [33])

Anisotropy	Uniaxial	Cubic, $K_1 > 0$	Cubic, $K_1 < 0$
M_r/M_s	0.5	0.832	0.866

13.4 Induced Magnetization and Domain Wall Motion

Coeroivities predicted for coherent rotation for iron, nickel and cobalt range from 2.5 to 850 kA m^{-1} but measured values, for presumed multidomain specimens, are usually orders of magnitude smaller than these. Calculated rotational susceptibilities are of the order of 10 to 100 compared to measured values up to 10^6 for single crystals of iron and measured remanences may be virtually zero. Domain wall processes are much 'easier' than rotation.

A field applied parallel to a 180° wall may be considered to exert a pressure on the wall

$$P_H = 2\mu_0 H M_s \tag{247}$$

in view of the change in energy as the wall moves. For a structure such as that shown in Figure 1.57(a) this may be balanced by a restoring pressure due to demagnetizing fields, but if the specimen becomes indefinitely elongated the latter becomes negligible and χ increases indefinitely. (This neglects the intrinsic wall coercivities which may exist even in perfect crystals if the walls are exceptionally narrow [23] and the continuum model is not fully applicable [34].) In general, if it is assumed that the wall remains plane it is easy to calculate and minimize the sum of E_m and $E_H = -\mu_0\mathbf{H}\cdot\mathbf{M}$ to give the equilibrium wall positions and magnetization. This gives the anhysteretic magnetization curve since the crystal is implicitly perfect with no variation in the domain wall energy with its position. $M_r = 0 = H_c$ and there is no hysteresis loss, defined by

$$W_H = \mu_0 \oint H\,\mathrm{d}M \tag{248}$$

around the 'loop'; this is the net work expended by the field in changing the magnetization which is equal to the area of the M/H loop (in this case zero).

If a specimen contains a large number of walls the magnetization may be taken to be homogeneous as an approximation. For an ellipsoidal specimen with low crystal anisotropy the induced magnetization and susceptibility are, as previously noted,

$$M = \frac{\chi H_a}{1+N\chi}, \qquad \chi_e = \frac{M}{H_a} = \frac{\chi}{1+N\chi} \to \frac{1}{N} \qquad (N\chi \gg 1)$$

Thus if $\chi = M/H$, with H the internal field, is high then the effective susceptibility is controlled by demagnetizing effects unless $N \to 0$.

In technical applications overall demagnetizing effects are avoided by assembling strips of material into rectangular frames, winding ribbons or tapes into toroids or producing toroids of sintered materials such as ferrites. The properties measured for such specimens can be taken to be characteristics of the material (and its particular microstructure), although some internal demagnetizing effects which arise where $\mathbf{M}_s$ changes in direction at grain boundaries may still be involved.

In such specimens, however, χ and $\mu_r = 1 + \chi$ may be controlled by impediments to free domain wall motion caused by any imperfections or irregularities that render the wall energy position-dependent. These include any variations in A or K or, more drastically, the presence of pores (or non-magnetic inclusions) or inclusions of foreign magnetic phases. A wall tends to remain in a 'trough' where its energy density is anomalously low or to be 'repelled' by regions where γ increases. A pore or inclusion reduces the local wall energy density by effectively removing a small area of the wall. Moreover, if a relatively large spherical inclusion is bisected by a narrow wall the associated magnetostatic energy is halved, since it is effectively an isolated sphere with M_s opposite to that of the surroundings, and this clearly impedes the wall.

The wall motion thus proceeds by a series of Barkhausen jumps between energy minima, and if the specimen loads a coil the effect will be the production of noise in the voltage generated. In a randomly oriented polycrystal only a certain fraction of saturation can be achieved by wall motion (corresponding to the remanence) and this must be followed by rotation. If a core is biased by a static field so that an a.c. field gives small excursions of the magnetization at a high level, it is found that the noise decreases, i.e. the signal-to-noise improves, although the susceptibility and signal per unit a.c. field amplitude falls.

Many materials may be expected to contain uniformly distributed inclusions, e.g. of iron carbide in iron, with narrow size ranges, and thus the field required to initiate wall motion will move the walls past successive inclusions. When a near-saturating field is removed and reversed this same characteristic 'wall-impedance field' magnitude will be required to cause demagnetization and thus constitutes the coercivity. This gives, for a grain-oriented specimen, a virgin curve from, say, an a.c. demagnetized state (achieved by gradually reducing the amplitude of an initially large a.c. field), and an M/H loop, somewhat as

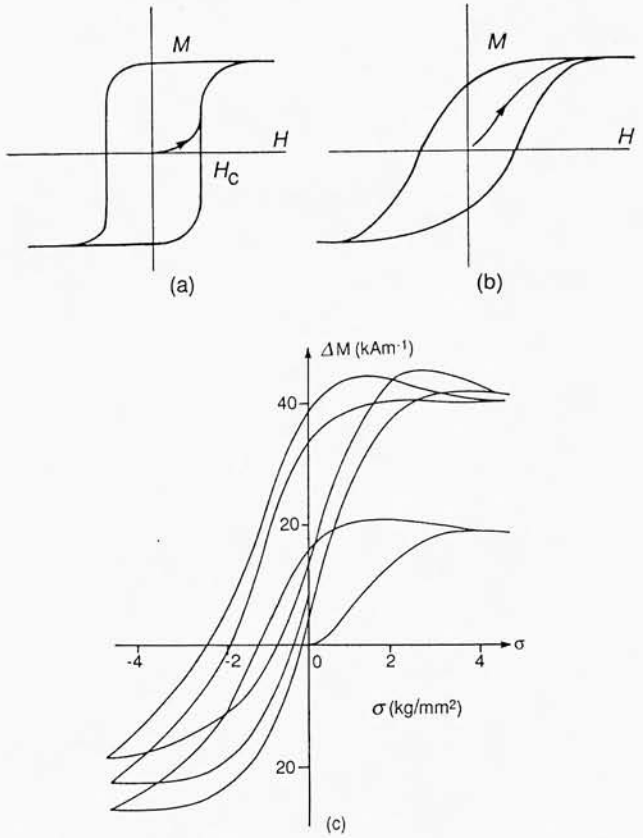

Figure 1.65 (a) The expectation for a grain-oriented material with a characteristic wall impedance field H_c and (b) a sigmoid loop for a randomly oriented polycrystal with rotational processes taking over at the higher fields; (c) indicates how applied tensile stresses may induce a magnetization, and remanence, in small fields [30]. Repeated stress cycles for random SiFe (3 per cent)

shown in Figure 1.65(a). The curvatures are due to (a) some variation in the wall impedance fields and (b) demagnetizing effects, both internal in association with grain boundaries and associated with small components of $\mathbf{M}_s$ across the external surfaces, since the orientation is never perfect. In such cases the following approximations obviously apply:

$$W_h \doteqdot 4\mu_0 H_c M_s$$
$$\chi_m \doteqdot \frac{M_s}{H_c} \tag{249}$$
$$\mu_r^m = 1 + \frac{M_s}{H_c}$$

with W_h the hysteresis loss per cycle and χ_m the maximum susceptibility, i.e. the tangent of the greatest angle of slope of the line drawn from 0 to points on the loop.

For randomly oriented polycrystals the loops are more as shown in Figure 1.65(b). The pronounced curvatures giving a typically sigmoid virgin curve are due, at low fields, to the existence of a range of wall pressures due to varying angles between the field and the walls and, at higher fields, demagnetizing effects and the merging of wall motion and rotational processes.

In the development of soft magnetic materials, with high permeabilities and low hysteresis, the main objectives are the elimination of features impeding wall motion or the reduction of their effectiveness. The first is achieved by purification and homogenization, as well as stress relief since local stresses cause variations in the total anisotropy. The second is achieved largely by minimizing the anisotropy, (and magnetostriction) as in Ni–Fe alloys or permalloys, to give minimal γ and very wide walls. The inclusions etc. may then be much smaller than the wall width and their effectiveness is reduced [35, 36]. In extreme cases the walls may occupy a substantial proportion of the specimen and the merging of the wall motion and rotation occurs at low levels of M, giving initial susceptibilities χ_i comparable to maximum susceptibilities. [For the loops in Figure 1.65(a) applicable to grain-oriented silicon iron, $\chi_i < \chi_{max}$.]

A wall impeded at a particular point will tend to be plucked like a bow string, but the curvature is opposed both by the increase in total wall energy and the introduction of magnetostatic energy due to the components of M_s across the wall. Thus the walls in high M_s, high γ materials such as SiFe tend to remain planar while those in very soft ferrites and alloys bow more readily.

If the crystallites are relatively free of imperfections but the walls are restricted at grain boundaries, either naturally due to magnetostatic effects or due to intergranular porosity etc., as occurs in ferrites, then the initial permeability may be largely associated with wall bowing. The greater the span the easier is the motion in relation both to the surface tension effect and the magnetostatic energy involved. It is frequently found that μ rises approximately linearly with grain diameter (see 2.3, Chapter 5).

One way to minimize the anisotropy is to reduce the grain size so extremely that, over a distance for which $\mathbf{M}_s$ is constrained to be nearly uniform by the exchange, the orientation of the crystal axes changes so that the anisotropy averages out, i.e. to produce nanocrystalline materials (see Chapter 5, Section 2.3.1, final part) or, ultimately, amorphous materials (Chapter 5, Section 2.3.1). There appears currently to be rather a contest between the development of these newer materials and the improvement of conventional materials.

The application of a tensile stress to a specimen in a field which itself gives little induced magnetization, e.g. the earth's field, may, by affecting the total anisotropies, favour the growth of certain domains and induce a substantial magnetization remaining, partially, as a remanence when the stress is removed (see, for example, [37, 38] and the theory of Brown [39]), as in Figure 1.65(c). Motor vehicles, ships and submarines acquire magnetic signatures which may be removed by elaborate 'de-Gaussing', and the historic production of compass needles by hammering in the earth's field doubtless depended on stress-induced magnetization.

13.5 Domain Nucleation

If complete saturation is attained a new problem arises since to achieve demagnetization new domains must nucleate and grow, though in many cases residual domains may persist in association with pores, defects on surfaces even when $M \to M_s$ closely, and the problem is then only apparent.

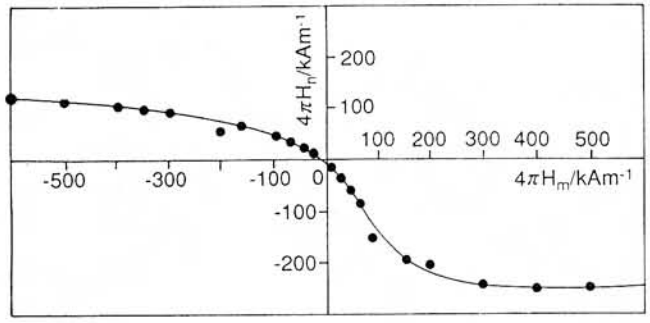

Figure 1.66 The dependence of the nucleation fields H_n in crystals of $EuFeO_3$ with damaged surfaces, on the magnitude of the saturating field and its direction, suggesting exchange coupling with foreign phases, exchange anisotropy (by C. Tanasoiu and the author)

Since the magnetization must reverse locally to form the nucleus of a 180° domain, for example, reverse fields of the magnitude of H_K would appear to be required. However, these would cause complete reversal by rotation and it is known that nucleation fields H_n are usually much lower than H_K; indeed, in many soft materials domains appear to nucleate spontaneously in zero reverse applied fields. A major factor appears to be the reinforcement of reverse applied fields by local stray or demagnetizing fields, including the effects of field components transverse to the applied fields and to M_s (see, for example, [40]).

In hard magnetic materials, permanent magnets, the coercivities may be controlled by extremely strong domain wall pinning due to deliberately contrived multiphase structures or fine precipitates, but in high-anisotropy single-phase materials H_c appears to be controlled by nucleation, as discussed in Chapter 5.

In a famous demonstration by Sixtus and Tonks [41] a wire of permalloy was stretched to give a stress-induced easy axis along its length ($\lambda_s > 0$). After saturation in a 'positive' direction the specimen remained saturated, $M_r = M_s$, even in small negative fields. However, when a negative pulse field was applied along a small length of the wire a domain was nucleated and a single wall swept along the wire to give a giant Barkhausen jump encompassing complete reversal, as inferred from the voltage pulses produced at different times in two pickup coils around the wire. Thus information was obtained both on nucleation and on domain wall velocities.

In certain cases the nucleation fields depend on the previously applied saturation fields, as originally demonstrated in orthoferrite crystals by the author and McIntyre [42] (Figure 1.66). This is associated with the presence of foreign phases formed during specimen preparation and identifiable by Faraday microscopy, exchange-coupled to the bulk. It is only as this material becomes saturated that the nucleation fields approach high values (see Chapter 6, Section 1). It has been suggested that related effects are important in a number of permanent magnet materials.

14 Classical Magnetization Dynamics

The principles governing the approach of **M** to its equilibrium magnitude and direction in an applied field, a state assumed in the foregoing treatments, are discussed in Chapter 3.

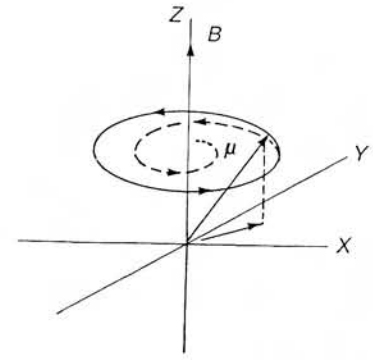

Figure 1.67 The (classical) precessional motion of an undamped spin or magnetic moment in an applied field with longitudinal and transverse components of constant magnitude. The broken line indicates the effect of damping

For a moment μ, e.g. **M** × volume for a single-domain particle, the undamped equation of motion is $d\mu/dt = \gamma\mu \times \mathbf{B}$ with **B** a field applied at an angle θ to μ. Solutions (for $\mathbf{B} \parallel OZ$) are shown to be $\mu_x = \mu \sin\theta \cos\omega_0 t$, $\mu_y = \mu \sin\theta \cos\omega_0 t$, $\mu_z = \mu \cos\theta$ = constant, where $\omega_0 = \gamma B$. The moment μ moves on a cone or precesses, at ω_0, and no magnetization is induced in the field direction. This is natural since energy changes consequent on changes in $\mu \cdot \mathbf{B}$ clearly require the introduction of damping or relaxations transferring energy to a reservoir or 'lattice'. When damping is introduced the precession is modified and μ spirals towards **B** (Figure 1.67). The gyromagnetic response arises from the inevitable association of angular momentum with μ or **M** and is thus a very basic feature of magnetic behaviour.

For single-domain particles or saturated specimens μ may be considered the total magnetic moment. Kikuchi [43] showed that the minimum switching time for reversal of the magnetization was $\tau_{min} = 2/(\gamma B_0)$ and that this was achieved by setting $\lambda = \gamma M_s$ with λ the damping parameter introduced by Landau and Lifshifz [25].

If a second smaller field is applied in the OXY plane and rotates in phase with μ at $\omega = \omega_0$ then it is conceivable that μ may be caused to approach the direction of B_0 with an energy change, giving a crude picture of ferromagnetic resonance as developed in Chapter 3.

For the dynamics of domain walls a familiar damped equation of motion may be used:

$$m\ddot{x} + \beta\dot{x} + \alpha x = 2M_s B(t) \tag{250}$$

with m the effective wall mass, β a damping coefficient, α a stiffness constant and the right-hand side the impressed periodic force. As a wall moves the spins rotate in a manner akin to precession in an effective field; the integral of the square of this field was used by Doring [44] and Becker [45] to calculate an excess wall energy proportional to $\dot{x}^2$ and an effective mass by equating this energy to $\frac{1}{2}m\dot{x}^2$. It can be shown that the damping (retarding) force is directly proportional to velocity if eddy currents control the damping. Finally, if $\ddot{x}$ and $\dot{x} \to 0$, $\alpha x = 2M_s B/A$, with A the total wall area, and since the induced magnetization is $M = 2M_s A x$, α can be related to the low-frequency susceptibility by

$$\alpha = 4\frac{\mu_0 M_s}{\chi} \tag{251}$$

The solution of the widely applicable equation (250) is standard. Clearly if $\beta = 0$ and the r.h.s = 0 the frequency of free oscillation is

$$\omega_0 = \sqrt{\frac{\alpha}{m}} \tag{252}$$

When $\beta \neq 0$ but $\beta^2 < 4\alpha m$ (and the r.h.s. is included), a resonant response occurs with peak absorption at

$$\omega = \left(\frac{\alpha}{m} - \frac{\beta^2}{4m^2}\right)^{1/2} \tag{253}$$

As β increases from a minimal value the resonance peak is first broadened and then disappears to be replaced by a gradual fall in the response, which is termed a relaxation.

When pulse fields of constant peak value are applied the acceleration period is usually negligible and the first term in equation (250) can thus be neglected. Once the walls have broken free from the impeding sites at $H = H_c$ the third term is irrelevant and the wall can be considered to move in the excess field according to

$$\beta\dot{x} = 2\mu_0 M_s(H - H_c), \qquad v = R(H - H_c) \tag{254}$$

with R the wall mobility. The switching speed depends on the number of walls but is inversely proportional to $(H - H_c)$: $\tau^{-1} = S(H - H_c)$.

15 High-Frequency Susceptibilities and Losses

The energy stored in a coil or inductor can be expressed in terms of the inductance L and current flowing i, or the fields, according to (Chapter 4, 1.8 and 1.11):

$$E_t = \tfrac{1}{2}\int \mathbf{B}\cdot\mathbf{H}\,\mathrm{d}v = \tfrac{1}{2}Li^2 \tag{255}$$

For the energy density E, assuming $B \parallel H$,

$$\mathrm{d}E = H\,\mathrm{d}B = \mu_0(H\,\mathrm{d}H + H\,\mathrm{d}M) \tag{256}$$

If $B = \mu H$ and μ is constant, $\mathrm{d}E = \mu H\,\mathrm{d}H$ and integrating as the field is built up from zero $E = \frac{1}{2}\mu H^2 = \frac{1}{2}BH$ with this restriction. The expression for $\mathrm{d}E$ takes account of the energy of the magnetization in the field and also shows that even in the absence of magnetizable material, i.e. in space or effectively in an air-filled coil, work must be done to create the field. However, this 'field term' is reversible and there is no associated net energy flow from a source to an inductor which presents an impedance but no effective resistance. The second term, $\mu_0 H\,\mathrm{d}M$, may also lead to reversible energy changes throughout a cycle with no net energy flow or losses if the magnetization is induced reversibly, but more generally the hysteresis loss per cycle [equation. (248)] is the area of the M/H loop ($\times\mu_0$) and in the general case is non-zero due to finite coercivity. Usually the term 'hysteresis loss' is confined to the loss for the quasi-static loop. As the cycle frequency increases the loops may be seen to expand, with additional high-frequency losses. Low-amplitude loops can frequently be approximated as

$$M = \chi_0 H \pm \tfrac{1}{2}\eta H^2 \tag{257}$$

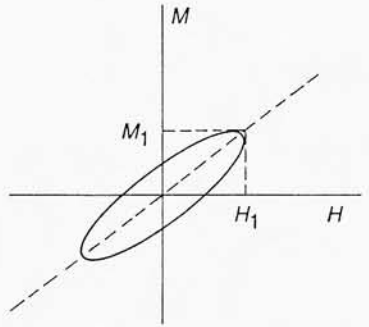

Figure 1.68 Approximated low-amplitude loop: $M = \chi_0 H \pm \frac{1}{2}\eta H^2$ with χ_0 the slope of the broken line and η an empirical Rayleigh constant. The loss is $\propto \eta H_1^3$

(see Figure 1.68) with χ_0 the anhysteretic initial susceptibility and η the Rayleigh constant. The hysteresis loss per cycle is then

$$\omega = \tfrac{4}{3}\mu_0^r \eta H_1^3 \tag{258}$$

with H_1 the field amplitude and μ_0^r the initial relative permeability.

It is clear by simple geometry that as loops resembling that in Figure 1.68 are traversed dynamically there must be a phase difference or lag δ between M and H as indicated by

$$\begin{aligned} H(t) &= H_0\cos\omega t \\ M(t) &= M_0\cos(\omega t - \delta) \\ &= M_0\cos\omega t\cos\delta + M_0\sin\omega t\sin\delta \\ &= \frac{M_0\cos\delta}{H_0}H_0\cos\omega t + \frac{M_0\sin\delta}{H_0}H_0\sin\omega t \\ &= \chi' H_0\cos\omega t + \chi'' H_0\sin\omega t \end{aligned} \tag{259}$$

defining

$$\chi' = \frac{M_0\cos\delta}{H_0}, \qquad \chi'' = \frac{M_0\sin\delta}{H_0} \tag{260}$$

In complex notation with $H(t) = H_0 e^{i\omega t}$, assuming that

$$\begin{aligned} M(t) = \chi H(t) &= (\chi' - i\chi'')H_0\,e^{i\omega t} \\ &= (\chi' - i\chi'')H_0(\cos\omega t + i\sin\omega t) \\ &= \chi' H_0\cos\omega t + \chi'' H_0\sin\omega t + i(\chi' H_0\sin\omega t - \chi'' H_0\cos\omega t) \end{aligned}$$

then the real part of M corresponds to equation (259). Thus χ' and χ'' can be interpreted as the real and imaginary parts of a complex susceptibility:

$$\chi = \chi' - i\chi'' = |\chi|e^{i\delta} = |\chi|\cos\delta - i|\chi|\sin\delta \tag{261}$$

with $|\chi|^2 = \chi'^2 + \chi''^2$.

The power loss per cycle per unit volume is

$$W_c = \int_0^T \mu_0 H \, dM = \int_0^T \mu_0 H \frac{dM}{dt} dt$$
$$= -\int_0^T \mu_0 \chi' H_0^2 \omega \cos \omega t \sin \omega t \, dt + \int_0^T \mu_0 \chi'' H_0^2 \omega \cos^2 \omega t \, dt$$
$$= \pi \chi'' \mu_0 H_0^2 \qquad (262)$$

over the cycle time $T = 2\pi/\omega$, the first term giving zero and the second evaluated as $(1/\omega)(\frac{1}{2}\omega t + \frac{1}{4}\sin 2\omega t)$. Thus the power loss per second per unit volume is

$$P = \tfrac{1}{2}\omega \mu_0 \chi'' H_0^2 \qquad (263)$$

This is clearly the a.c. power loss since $P \to 0$ as $\omega \to 0$, explicitly and because $\chi'' \to 0$ also, as $\delta \to 0$, and it is assumed that M follows H exactly at its equilibrium value. Thus $\chi_0 = M_0/H_0$ is the anhysteretic initial susceptibility. Such treatments are usually taken to apply specifically to initial susceptibilities or the corresponding initial permeabilities.

If a zero-resistance air-filled coil has inductance L_0 then $L = \mu L_0$ when it is filled by a core of constant permeability μ. When the permeability is complex the complex impedance is

$$Z = R + iX = i\omega L_0 \mu = i\omega L_0 \mu' + \omega L_0 \mu''$$
$$R = \omega L_0 \mu''$$
$$X = \omega L_0 \mu'$$

with R the resistive and X the reactive component of the impedance.

Plots of μ'' and μ' against frequency are termed permeability spectra and examples are given in Figures 1.71 and 5.18. They may be indicative of so-called relaxations with gradual fall of μ' and rising μ'' or of resonances with a peak in μ'' as μ' falls rapidly (although relaxation is also, of course, involved in the latter). The resonances require the existence of restoring torques or forces as afforded by anisotropy. The relaxations may be associated with the diffusion of carbon atoms in iron or the diffusion or hopping of electrons between ferrous and ferric ions in ferrites, and these may also lead to magnetic after-effects, an appreciably slow approach to the equilibrium magnetization, and disaccommodation of the permeability, slow decreases in the real part being due to the progressive stabilization of certain states of the magnetization by the diffusion. In very highly insulating oxide materials with minimal Fe^{2+} content the formation of spin-waves coupling directly to the lattice vibrations (phonons) is invoked.

16 Eddy Currents

In metals and relatively highly conductive oxide materials, eddy current losses are expected to predominate. Empirically the major distinction is that eddy current losses depend strongly on the specimen dimension: strip or sheet thickness or powder particle size. Eddy current effects are not unique to, but are enhanced in, magnetic materials and form the basis of induction heating, techniques from the surface tempering of steels to delicate medical treatments.

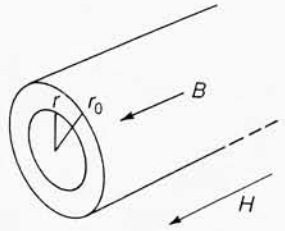

Figure 1.69 Construction for eddy currents in a cylinder

Applying the relation for the electric field E, which derives from Maxwell's laws:

$$\oint E_l \, dl = -\int\int \frac{dB_n}{dt} dS \qquad (264)$$

to the infinitely long cylinder of Figure 1.69 gives

$$2\pi r E(r) = -\pi r^2 \frac{dB}{dt}, \qquad \text{i.e. } E(r) = -\frac{r}{2}\frac{dB}{dt} \qquad (265)$$

The surface integral applies to the area enclosed by the radius r and it is assumed as a simplifying approximation that dB/dt is uniform. The induced current is

$$i(r) = \frac{E(r)}{\rho} = -\frac{r}{2\rho}\frac{dB}{dt} \qquad (266)$$

with ρ the resistivity. The power loss in an annulus between r and $r + dr$ is $Ei(2\pi r \, dr)$ per unit length of the cylinder. Integrating, the instantaneous loss per unit volume is

$$P = \frac{1}{\pi R^2}\int_0^R \left(-\frac{r}{2}\frac{dB}{dt}\right)\left(-\frac{r}{2\rho}\frac{dB}{dt}\right) 2\pi r \, dr$$
$$= \frac{1}{2\rho R^2}\left(\frac{dB}{dt}\right)^2 \int_0^R r^3 \, dr = \frac{R^2}{8\rho}\left(\frac{dB}{dt}\right)^2 = \frac{R^2}{8\rho}\mu^2\left(\frac{dH}{dt}\right)^2$$

Integrating over a cycle with $H(t) = H_0 \cos \omega t = H_0 \cos 2\pi f t$, the mean power loss becomes

$$\bar{P} = \frac{\pi^2 R^2 \mu^2 f^2 H_0^2}{4\rho} \qquad (267)$$

This is quoted by Smit and Wijn [46] for example who also gave

$$\bar{P} = \frac{2\pi^2 R^2 \mu^2 f^2 H_0^2}{3\rho} \qquad \text{(plate, thickness } R\text{)} \qquad (268)$$

$$\bar{P} = \frac{\pi^2 R^2 \mu^2 f^2 H_0^2}{5\rho} \qquad \text{(sphere, radius } R\text{)} \qquad (269)$$

(The expressions quoted by Smit and Wijn contained a factor of 10^{-16} to give the quantity in W cm^{-3} when H is taken to be in Oe and ρ in Ω cm, but such factors are unnecessary in the SI and the losses are automatically given in W m^{-3}, remembering that $\mu = \mu_r \mu_0$.) The losses are now dependent on ω^2, rather than ω, and the dependence on the square of the characteristic dimension is introduced.

The losses as calculated above are usually found to be too low by a factor of about 3 since homogeneous magnetization was assumed and in practice intense losses are associated with moving domain walls, except at extremely high frequencies, at which the walls are effectively demobilized by these effects and (homogeneous) rotation takes over. The magnitude of the anomaly depends on the widths and spacings of the walls and these are usually unknown.

It may be repeated that in the foregoing dB/dt, and by implication B, was taken to be independent of r, i.e. uniform throughout the cylinder. This will never be wholly true. In a thin annular skin on the outside of the cylinder H can be identified with the applied field due to the continuity of the tangential component. The currents induced in this annulus create a reverse field within (and only within) this annulus which detracts from the applied field and thus the penetration of the field is limited. The equation governing the field is

$$\nabla^2 \mathbf{H} = \frac{\mu}{\rho} \frac{d\mathbf{H}}{dt} \tag{270}$$

which may readily be solved in the one-dimensional case (Figure 1.70) assuming the usual separation $H = f_1(t) \times f_2(y)$ with boundary conditions corresponding to $H = H_0 e^{i\omega t}$ at the surface, $y = 0$:

$$H = H_x(y, t) = H_0 e^{-\alpha y} e^{i(\omega t - \alpha y)}, \qquad \text{where } \alpha = \sqrt{\frac{\mu_r \omega}{2\rho}} \tag{271}$$

The frequency is unchanged but a phase shift proportional to y is introduced. The magnitude decreases exponentially within the material and H is virtually excluded for y substantially greater than α. A skin depth δ is defined as that at which the amplitude is reduced by $1/e$:

$$\alpha\delta = 1, \qquad \text{i.e. } \delta = \sqrt{\frac{2}{\mu_r \omega}} \tag{272}$$

e.g. at 50 Hz for silicon iron, $\delta \approx 1$ mm, which is much less than the value for copper (≈ 10 mm) with a lower value of ρ ($2 \times 10^{-10} \Omega$ m) but $\mu_r = 1$. The currents may be shown to behave in a similar manner:

$$i = i_z = i_0 e^{-\alpha y} e^{i(\omega t - \alpha y)}$$

and the power loss per unit surface area may be obtained by integration as

$$P = \tfrac{1}{2} \sqrt{\frac{\mu\omega\rho}{2}} \bar{H}_0^2 \tag{273}$$

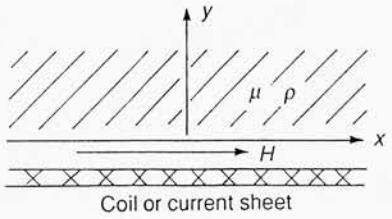

Figure 1.70 The tangential field H must be the same just inside the material but then falls off exponentially

with $\bar{\mathbf{H}}_0$ the r.m.s. value. It may also be seen that the dissipation is very non-uniform and that, for example, selective surface heating of steels may be achieved in an important technical application. Full analyses can also be made for plates of finite thickness and for cylinders: with cylindrical symmetry the diffusion equation becomes Bessell's differential equation and the results are obtained as Bessell functions.

It is now seen that the simple results given in equations (267) to (269) apply for $R < \delta$ substantially, so that uniform penetration of the field may be assumed.

The governing equations have the form of the diffusion equation. Since the functional for the diffusion equation is known this may be solved numerically by the finite element method (see Section 4.3, Chapter 5) and a very substantial literature on this may readily be located in the obvious journals. (The time-dependent Schrodinger equation has the form of the diffusion rather than the wave equation and the author has found the solution of this to be straightforward.)

In the usual case the objective is to reduce eddy current losses by the use of thin strips (in the past by introducing wires or metal powders) or, of course, by attention to the resistivity values of metals or the substitution of metals by the relatively insulating oxides or ferrites. (For ferrites ρ ranges from 10^5 for $MgFe_2O_4$ through ~ 10 for NiZn ferrites to $10^{-5} \Omega$ m for Fe_3O_4.) However, eddy currents may be viewed more positively with applications for induction heating ranging from metallurgy to medicine.

The treatments of relaxation/resonance losses and eddy current losses are distinct. The former depend on the material and the latter depend also on the geometry. The use of complex permeabilities is not appropriate for eddy currents since the phase lag varies spatially. The short-range motion of electrons in the hopping mechanism must be distinguished from the long-range motion giving the extensive currents assumed in the eddy current analyses, but if the activation energy for hopping is progressively reduced the two

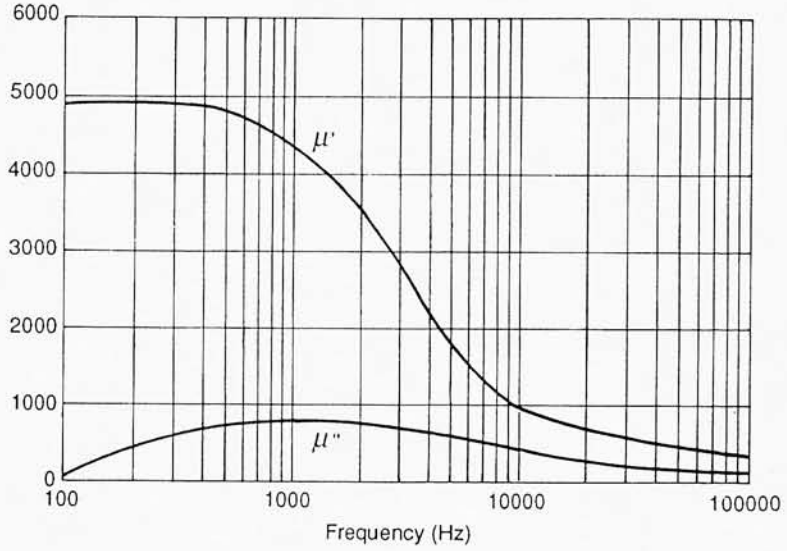

Figure 1.71 The real and imaginary parts of the permeability for a magnetite single crystal; typical relaxation effects as opposed to resonant absorption [47] (cp Figure 5.18)

approaches may be imagined to merge. Rather remarkably Galt [47] interpreted the losses in Fe_3O_4 crystals, as indicated by Figure 1.71, in terms of relaxation and calculated that the eddy current effects were virtually negligible. However, eddy current losses are considered to be appreciable in commercial MnZn ferrites, which contain ferrous ions to reduce the anisotropy and increase the low-frequency permeability at the expense of the useful frequency range, with $\rho = 10^{-3}$ to 10^{-4} Ω m. Due to this, reoxidation is used to give layers of Fe_2O_3 at the grain boundaries, or impurities such as calcium are introduced, which segregate at the grain boundaries and form insulating layers.